Polymer Chemistry

RSC Publishing

REVIEW

View Article Online
View Journal | View Issue

Cite this: *Polym. Chem.*, 2013, **4**, 211

Functional polyacetylenes: hybrids with carbon nanotubes

Jing Zhi Sun,*[a] Anjun Qin[a] and Ben Zhong Tang*[ab]

Functional polyacetylenes (PAs) have attracted great interest and a series of tutorial reviews dealing with the recent progress in the related fields can be found in the literature. The investigation of the hybrids of functional PAs and inorganic nanostructures is a newly asserted and developing area. In this review, we summarise the related works on the hybrids of functional PAs and carbon nanotubes (CNTs) reported in the last decade. The effects of the structural parameters such as the polymer mainchain, functional pendants and the linker between them on the solvating power towards CNTs are explored step-by-step. Concerning the mechanisms of dispersing CNTs into solvents, a novel factor, or donor–acceptor interaction, has been singled out, thus providing a novel concept to design functional polymers for the fabrication of CNT-based processable hybrids. The strong solvating power of properly designed functional PAs facilitates the non-harmful surface functionalization of CNTs and permits using the hybrids of PAs/CNTs as templates to derive multi-component nanocomposites. Different nanostructures including Ag nanoparticles, ZnO nanocrystallites, CdS nanorods and γ-Fe_3O_4 nanoparticles are successfully incorporated into the functional PAs/CNTs hybrid systems, which show efficient charge transfer, charge carrier transport, enhanced solvatochromism, and superparamagnetic properties. Rationally functionalized PAs demonstrate good biocompatibility and their hybrids with CNTs can be used as active additives to reinforce the bending strength and modulus of chitosan rods. Finally, a brief outlook of the promising directions in this promising research area is contributed.

Received 2nd July 2012
Accepted 11th August 2012

DOI: 10.1039/c2py20469j

www.rsc.org/polymers

[a]*MOE Key Laboratory of Macromolecular Synthesis and Functionalization, Department of Polymer Science and Engineering, Institute of Biomedical Macromolecules, Zhejiang University, Hangzhou 310027, China. E-mail: sunjz@zju.edu.cn; Fax: +86-0571-87953734; Tel: +86-0571-87953734*

[b]*Department of Chemistry, Institute for Advanced Study, Institute of Molecular Functional Materials, State Key Laboratory of Molecular Neuroscience, and Division of Biomedical Engineering, The Hong Kong University of Science & Technology, Clear Water Bay, Kowloon, Hong Kong, China. E-mail: tangbenz@ust.hk; Fax: +86-852-2358-7375; Tel: +86-852-2358-1594*

Jing Zhi Sun received his B.S. degree and PhD degree from the Department of Chemistry at Jilin University in 1986 and 1999, respectively. He conducted his postdoctoral research at Zhejiang University (ZJU) and jointed ZJU in 2001 as an assistant professor, then became a full professor in 2006. His current research interests include conjugated polymers, polymer hybrids and bioelectronics based on aggregation-induced emission luminogens.

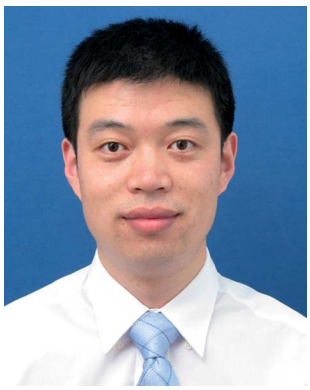

Anjun Qin received his Ph.D. degree in Physical Chemistry from Institute of Chemistry, Chinese Academy of Sciences in 2004. From 2005 to 2008, he worked as a postdoctoral associate in Tang's laboratories at HKUST and Zhejiang University. He was promoted to Associate Professor at Zhejiang University in December 2008. He is interested in the construction of linear and hyperbranched polymers from triple-bond building blocks, especially the exploration of new catalyst systems and the development of new polymerization reactions.

1 Introduction

Polyacetylene (PA) is the prototype conjugated polymer, and its doped form is considered to be the first "synthetic metal".[1–3] Recently, PA has been appreciated to be the "First Generation" of semiconducting polymers.[4] Accompanied by the development of semiconducting polymers into the "Third Generation", PA derivatives have also demonstrated versatile and advanced functions for electronic, optical, supramolecular, and biological materials which retain the attractive mechanical properties and processing advantages of polymers. For example, it once was a general concept that a conjugated polymer bearing mesogens in its side chains could hardly possess liquid crystal properties because the rigid mainchain may distort the packing of the mesogens. But some elegantly designed PAs showed good liquid crystallinity, in which the whole polymer chains play the role of mesogens and the rigidity of the conjugated mainchains have a positive effect on inducing anisotropic alignments during the formation of mesophases.[5–7] According to quantum theory, PA is non-emissive due to its intrinsic electronic structure.[8] By appropriate substitution of the acetylene monomers, the resultant PAs exhibit modified intrachain electronic coupling and distinct electronic interactions of the polyene chains; thus, fluorescence from the pendant, the backbone, or both of them has been observed.[9–11] More recently, it was found that the fluorescence intensity of disubstituted polyacetylenes is evidently boosted in their aggregated states in comparison with in their dilute solutions or at lowered temperature.[12,13] This is a typical phenomenon of aggregation-induced emission enhancement, which is helpful to tackle the thorny problem of aggregation-caused fluorescence quenching observed for classical fluorescent polymers by rational structure design. Since Tang and Kotera pioneered the work on optically active PAs in 1989,[14] a variety of helical PAs have been derived by rationally attaching chiral centers to the side chains, which result in chirality in the polyene backbone and result in the formation of one-handed helicity.[15,16] Meanwhile, the synthesis of helical PAs using a chiral nematic liquid crystal reaction field as an asymmetric polymerisation is progressing in parallel.[17,18] In addition, the fabrication of carbon and graphitic films bearing completely preserved morphologies and even helical nanofibril structures using helical PAs as a carbonization precursor has become an attractive area since the original work reported by Akagi and colleagues.[19]

In the past decades, there has been impressive progress in the synthetic strategy, functional design, and materials applications of PA derivatives.[20–30] In pursuing high materials performance, hybridization of conjugated polymers with inorganic components has been extensively explored. By fine tuning the chemical functionality, polymer structure, size, morphology and composition of the inorganic nanostructures, hybrid materials are expected to show synergistic properties over each individual hybrid component and even new phenomena. Integrating flexible and easily functionalizable polymeric units with mechanically rigid and stable inorganic units offers broad processability and applications. Quite a few comprehensive and tutorial reviews on the relevant topics can be found in the literature.[31–35] However, there are no reviews on the hybrids of PAs with inorganic materials. Herein, we contribute a brief summary of the recent progress on nanohybrids composed of functional PAs and inorganic nanostructures.

Ben Zhong Tang received his B.S. degree from South China University of Technology and his Ph.D. degree from Kyoto University. He conducted postdoctoral research at University of Toronto and worked as a senior scientist in the central laboratory of NEOS Corp. He joined the Department of Chemistry at The Hong Kong University of Science and Technology as an assistant professor in 1994 and was promoted to chair professor in 2008. He was elected to the Chinese Academy of Sciences in 2009. He received a Natural Science Award from the Chinese Government in 2007. He is currently serving as Editor-in-Chief of RSC Polymer Chemistry Series (Royal Society of Chemistry) and Editor of Polymer Bulletin (Springer).

2 Hybrids of functional PAs and CNTs

Carbon nanotubes (CNTs, including multiwalled nanotubes or MWNTs and single-walled nanotubes or SWNTs) are of great interest in scientific research and technological innovation due to their unique nanostructures and novel materials properties, especially their remarkable electronic and optical properties. Several issues have to be addressed before CNTs can be integrated into functional hybrids for the fabrication of advanced materials and devices. One of the most challenging problems is their notorious intractability: CNTs are insoluble in any solvents and infusible at any temperature before decomposing. The approach of noncovalent functionalization by using conjugated polymers to improve the processability of CNTs seems to be a particularly attractive one because it does not damage the intrinsic electronic structure and properties of CNTs.[36–38] On the one hand, wrapping CNTs with conjugated polymer chains can endow the hybrids with processability and new photoelectronic properties. On the other hand, CNTs can help to enhance the charge transport, electrical conduction, optical nonlinearity, mechanical strength, and chemical stability of the hybrids.

2.1 Effect of structure parameters of functional PAs on solvating power towards CNTs

The first attempt to disperse CNTs in organic solvents by PA was reported by Tang and Xu in 1999.[39] *In situ* polymerization of phenylacetylene in the presence of CNTs gave rise to soluble nanohybrids of polyphenylacetylene (PPA) and CNTs. The hybrids demonstrated a high capacity for nonlinear attenuation of the incident laser pulses.

This work triggered the further exploration of processable hybrids of polymer-CNTs. Later on, disubstituted PAs were covalently bound to CNT shells and the resulting hybrid also showed the expected optical limiting properties.[40] To carry forward the advantages of noncovalent functionalization and consider that fused ring aromatics (*e.g.* pyrene) have been widely used as effective agents to help dissolve CNTs in organic solvents,[41–45] we designed and synthesized pyrene-functionalized PPAs.[46] The structures of the monomers and polymers are displayed in Chart 1 and their solvating power towards CNTs is shown in Fig. 1.

The experimental results (data in Fig. 1) disclosed the following information. Firstly, the polymers show much higher solvating power towards CNTs than their corresponding monomers (**P1** *vs.* **M1** and **P2** *vs.* **M2**). This can be defined as the "polymer effect". This effect, in some cases such as fluorescence enhancement and quenching, is also referred to as "super-amplification". Secondly, the solubility of a polymer has important effects on the solvating power towards CNTs (**P3** *vs.* **P4**). **P3** itself has a very low solubility in tetrahydrofuran (THF), thus it has no effect on the dispersion of CNTs in THF solution, while poly(phenylacetylene-*co*-**M3**) (**P4**) which is highly soluble in THF possesses the highest solvating power towards CNTs among the polymers shown in Chart 1. Thirdly, the pyrene-functionalized PPA shows better performance than the pyrene-functionalized polystyrene which has saturated main-chains (**P2** *vs.* **P5**).[45] This observation implies that the conjugated backbone plays an important role in the scenario of dispersing CNTs into solution. Finally, the pyrene-functionalized PPA demonstrates a very strong solvating power in that the hybrid of **P1**/CNTs has a solubility as high as 575 mg L^{-1} in THF. This value is over 3- and 11-fold higher than the pyrene-containing small molecules (**M1**–**M3**) and pyrene-functionalized co-polystyrene (**P5**), indicating that there is a pronounced "synergetic effect" of the PPA skeleton and the pyrene pendant.

The maximum solubility was recorded for the hybrids of the copolymer **P4**/CNTs, which is 637.5 mg L^{-1} in THF. At that time,

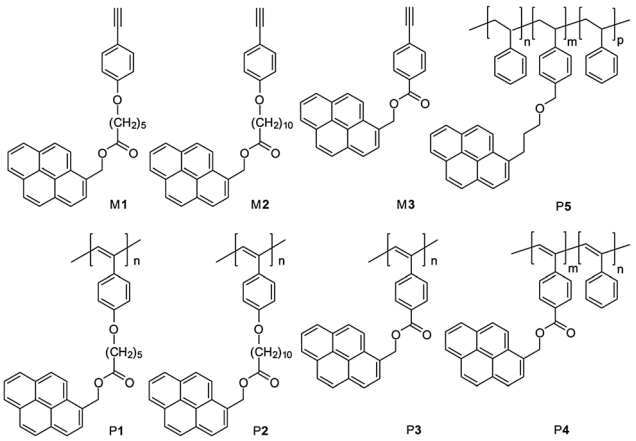

Chart 1 Chemical structures of a series of pyrene-functionalized phenylacetylene monomers, the corresponding polymers (**P1–P3**) and the poly(phenylacetylene-*co*-M3) (**P4**). The chemical structure of a **P4** analogous polystyrene derivative (**P5**) is also presented for comparison.

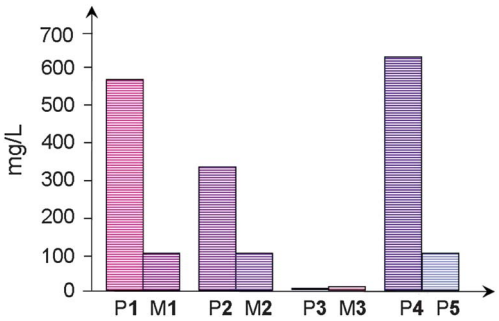

Fig. 1 The solvating power of functional PPAs (**P1–P4**, in Chart 1). The data for the corresponding monomers **M1**, **M2** and **M3**, as well as a pyrene functionalized polystyrene (**P5**) are also presented here for comparison.

this was the highest among all the solubility data reported for CNTs functionalized by small pyrene rings and wrapped by pyrene-containing polymer chains. This success indicates that functional PAs can be a class of promising polymers to fabricate soluble CNT-based hybrids. Meanwhile, it also initiates a chain of further research topics. In polymer chemistry, for instance, an important topic is how to systematically evaluate the effects of structural parameters (such as main-chain, functional pendants, and the linker between them) on the solvating power towards CNTs. We first examined the effect of the main-chain through a comparative investigation. As shown in Fig. 1 and 2, the hybrid of **P1**/CNTs has a solubility of 575 mg L^{-1} in THF, while that of **P6**/CNTs is only 467 mg L^{-1} under the same conditions.[47] This observation has been interpreted as following. Comparing **P2** with **P6**, the most striking difference in chemical structure is the polymer main-chain (Charts 1 and 2). For **P2**, a phenyl group is directly conjugated with a repeat unit of the polyene, but for **P6**, there is a sole polyene main-chain. It is believed that the pristine PA has a planar structure, irrespective of *cis* and *trans* configurations, due to the strong π-conjugation between the sp^2-hybridised carbon atoms in the polyene chain.[48,49] Substitution of PA reduces the strong inter-chain π–π interactions, thus making the PA derivatives soluble in solvents. Meanwhile, it has broken the planar structure of the main-chain in the substituted PA. Especially in the case of Rh-catalyst polymerization, the derived substituted PAs generally have a *cis*-rich configuration.[23,50–52] With their aromaticity, the phenyl groups in PPA, on the one hand, enlarge the

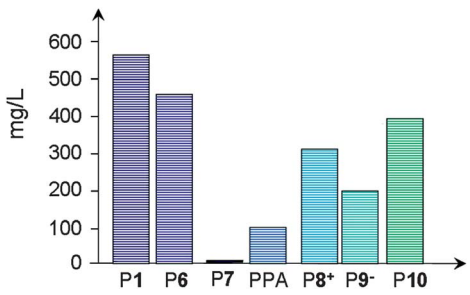

Fig. 2 The solvating power of functional PAs/PPAs (**P6–P10**, in Chart 2). The datum for **P1** is also presented here for comparison.

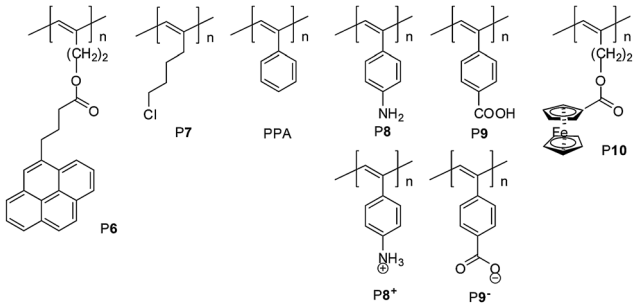

Chart 2 Chemical structure of a series of specially designed functional polyacetylenes (PAs).

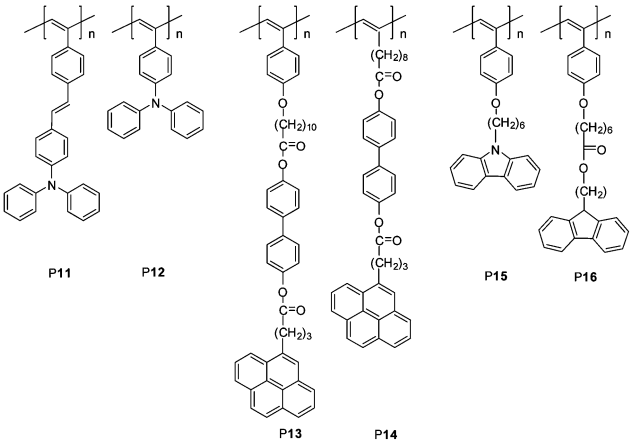

Chart 3 Chemical structures of functional PAs for demonstrating the effect of the linker and the role of D–A interactions.

π-conjugation system of the polymer chain and enhance the π–π interactions with CNTs, and on the other hand, the phenyl groups, with a more bulky size compared to methylenes, increase the probability of a helical conformation and facilitate the wrapping of the polymer chains onto the surface of CNTs. A more straight-forward proof comes from the comparison of PPA and **P7**. Without the help of phenyl groups, the polyalkyne (**P7**) showed very limited solvating power towards CNTs, but PPA has a solvating power of 100 mg L^{-1} in THF.[53] Moreover, as shown in Fig. 2 and Chart 2, PPAs with amino- (**P8**) and carboxyl (**P9**) functionalities also exhibit solvating power towards CNTs in appropriate solvents, and the solvating power of $\mathbf{P8}^{+}$ and $\mathbf{P9}^{-}$ towards MWNTs in water are 316 and 200 mg L^{-1} in acidic and basic conditions, respectively.[53] Consequently, PPA derivatives are preferred in our investigation of the hybrids of functional polyacetylenes and CNTs.[54–63]

The second structure parameter is the functional pendant of the PAs. Comparing the solubility data of **P7**/CNTs (undetectable) with **P6**/CNTs (467 mg L^{-1}) hybrids (Fig. 2), the effect of the pendant on the solvating power towards CNTs is quite pronounced. Accordingly, a series of different aromatic pendants have been examined. For example, ferrocene was used as a representative of aromatic pendants to be attached to the side chain of PA. The resultant **P10** demonstrated the expected solvating power towards CNTs and the solubility was measured to be 400 and 197 mg L^{-1} for the hybrids of **P10**/MWNTs and **P10**/SWNTs, respectively.[54] Besides ferrocene, the same strategy has been applied to the synthesis of functional PPAs bearing different pendants such as naphthalene, fluorene, carbazole, and triphenylamine and the fabrication of their hybrids with CNTs.[55,58,64] Based on the summarization of the data in Fig. 1 and 2, it can be found that, in general, the aromatic pendant with a larger π-conjugation system shows a higher solvating power (**P10** *vs.* **P6**).[57] This is a useful criterion for developing functional PAs and other polymers aimed at achieving desirable solvating power towards CNTs.

As the third structure parameter, the linker between the polymer mainchain and the functional pendant also plays a delicate role. In the same solvent and polymer concentration, **P1** has a stronger solvating power than **P2**. The longer flexible alkyl spacer may alienate the pyrene moieties from the polymer mainchain, thereby impairing the π–π interactions between the pyrenes and CNTs, which leads to the lower solvating power of **P2**. In the case of triphenylamine-functionalized PAs (**P11** and **P12**, Chart 3), the linker between the triphenylamine pendant and the polyene backbone has a distinct function.[55] **P11** is provided with an evident higher solvating power towards MWNTs than **P12**. Viewing their chemical structures, this difference between **P11** and **P12** can mainly be ascribed to the linking mode. The more flexible ethenoid linker not only extends the conjugation of the polyene mainchain and the triphenylamine pendants but also is favourable for the interactions between the triphenylamine moieties and MWNTs. In addition to the determination of the solubility of PAs and the distance between the mainchain and pendant, the effect observed for **P11** and **P12** suggests that the linker can be endowed with a certain function. Inspired by this idea, as shown by the chemical structure of **P13** and **P14**, a mesogen (biphenyl moiety) was inserted between the PPA chain and the pyrene groups, and flexible alkyl spacers were introduced into the polymer design to ensure the solubility of the polymers. As expected, both **P13** and **P14** demonstrated very high solvating power towards MWNTs and the solubility of the hybrid **P13**/MWNTs (625 mg L^{-1}) in THF is even better than that recorded for hybrid **P1**/MWNTs (575 mg L^{-1}) (Fig. 3). Moreover, because of the existence of biphenyl mesogen, the hybrid **P13**/MWNTs displays liquid crystal behavior that is similar to its polymer parent. Fig. 4 displays the polarized optical microscopic

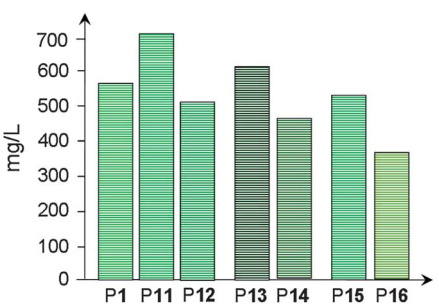

Fig. 3 The solvating power of functional PPAs (**P11–P16**, in Chart 3). The datum for **P1** is also presented here for comparison.

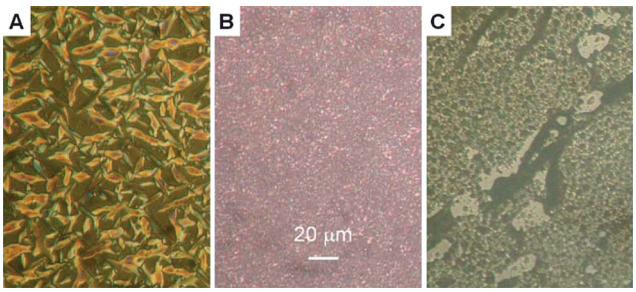

Fig. 4 Mesomorphic textures observed on cooling (A) **P13** to 150 °C, (B) **P14** to 165 °C, and (C) **P13**//-MWNT to 150 °C from their isotropic states at a cooling rate of 3 °C min^{-1}. Reproduced with permission from ref. 57. Copyright (2009) American Chemical Society.

photographs of the textures of **P13**, **P14**, and hybrid **P13**/MWNTs recorded in the heating–cooling cycles.[57] The hybrid is also mesomorphic, but the alignment and packing of the mesogens are worse than those in the pure polymer because MWNTs hamper the growth of the anisotropic domains. Accordingly, the differential scanning calorimetric data reveal that the *i*-SmA and SmA-*g* transition temperatures of the nanohybrid are lower than its pure polymer.

The effects of the polymer mainchain and the functional pendants on the solvating power towards CNTs observed for the monosubstituted PAs also occur for disubstituted PAs. In comparison with other conjugated polymers, using functional PAs to prepare CNT-based hybrids has some advantages. For example, it is easier to separately evaluate the contributions to the solvating power of the polymer main-chain and side-chains. This essentially comes from the good availability of functional acetylene monomers and facile polymerization procedures. In addition, mono-substituted PAs usually have a high *cis* content and the polymer mainchain predominantly takes on a helical conformation, which is propitious for wrapping the polymer chains onto the surface of CNTs and results in a strong solvating power towards CNTs. It is also worthy of mention that the hybrids of disubstituted PAs and CNTs retain a large portion of the fluorescence from the disubstituted PA component, suggesting that the hybrids can be potentially used as hybrid nanomaterials for fluorescent detection and sensors.[59,64]

2.2 Recognition of the role of donor–acceptor interactions between functional pendant and CNTs

There are mainly three well-accepted mechanisms of dispersing CNTs in different solvents with the aid of polymers, which are (i) π–π interactions, (ii) van der Waals interactions (*e.g.* hydrophobic–hydrophilic interactions), and (iii) electrostatic interactions between the polymers and the CNTs. As mentioned above, we have observed that the polymer chain wrapping around the CNT surface and the π–π interactions between the conjugated pendants and the CNT wall work synergistically to realize a high solvating power of functional PPAs towards CNTs in organic solvents.

By carefully analyzing the data presented in Fig. 2 and 3, some subtle discriminations can be found. For example, with the same polymer mainchain, the ionized amino-functionalized PPA (**P8**$^+$) shows stronger solvating power towards MWNTs than the ionized carboxylic-functionalized PPA (**P9**$^-$).[53] We initially ascribed this observation to the electron-withdrawing effects of the carboxylic group, which decreased the electronic density of the PPA backbone, thereby leading to the decrease in π–π interactions between the polymer mainchains and the MWNTs. But there might co-exist other factors such as the MWNTs favouring cations over anions and the counterions over the ammonium on **P8**$^+$ and the carboxyl on **P9**$^-$. Thus, the difference in solubility between **P8**$^+$/MWNTs (316 mg L^{-1}) and **P9**$^-$/MWNTs (200 mg L^{-1}) cannot be simply ascribed to the electronic effects at this stage.

A nontrivial observation came up in the experiments of dispersing MWNTs with triphenylamine-functionalized PPAs.[55] **P11** demonstrates a higher solvating power towards MWNTs than **P1** and **P13**. Generally, pyrene is believed to be a larger and better planar π-conjugate system than triphenylamine, thus it should perform better than triphenylamine for solvating MWNTs when pyrene and triphenylamine moieties were linked to an identical polymer backbone. Accordingly, the observed stronger solvating power of **P11** over **P1** and **P13** is somewhat "abnormal". To elucidate the underlying mechanism of the phenomenon, a tentative hypothesis of donor–acceptor (D–A) interactions between triphenylamine and MWNTs was proposed, considering that triphenylamine and MWNTs are well-known electron donors and acceptors, respectively. If the D–A interaction mechanism is true, the following experimental phenomena could be foreseen.

(i) Solvatochromism. Since MWNTs act as an acceptor, the intermolecular charge transfer from triphenylamine to MWNTs should be detectable. To verify this assumption, we investigated the solvatochromism of **P12** and **P12**/MWNTs. **P12** shows a weak solvatochromic effect because it is not a D–π–A structure (Chart 3). An evident solvatochromism, however, has been observed for the **P12**/MWNT hybrid (Fig. 5A and B). The

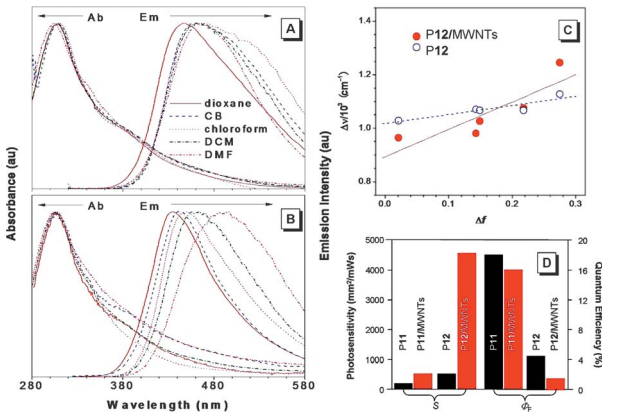

Fig. 5 (A) and (B) are the absorption (Ab) and emission (Em) spectra of **P12**, and **P12**/MWNTs hybrid in different solvents. (C) The Lippert–Mataga plot for **P12**/MWNTs and **P12**; (D) fluorescence quantum efficiency and photosensitivity of the photoreceptors using **P11**, **P12**, and **P11**/MWNTs, **P12**/MWNTs hybrids as CGM, respectively. Adapted with permission from ref. 55. Copyright (2009) American Chemical Society.

fluorescence spectrum of the **P12**/MWNT hybrid progressively shifts towards red with the increase in the solvent polarity; the emission maximum (λ_{em}) shifts from 434.0 to 500.0 nm when the solvent is changed from dioxane to DMF. The slope of the Lippert–Mataga plot for **P12**/MWNTs is larger than that for its parent polymer **P12**.[59]

(ii) Photoinduced charge transfer. Photoinduced charge transfer is another earmark of a D–A system; thus it is rationally used to verify the D–A interactions between the polymer and the MWNTs. We fabricated single-layered photoreceptors using the triphenylamine-containing PPAs and their MWNT hybrids as charge-generation materials (CGMs) and the photoconduction performance (evaluated by photosensitivity S) of the devices was measured with a standard GDT-II photoinduced discharge instrument.[65–67] The photoreceptor with **P11** as CGM shows a worse photoconductivity (S = 178.3 mm^2 mW^{-1} s^{-1}) than the device based on **P12** (S = 1010.1 mm^2 mW^{-1} s^{-1}). This can be explained as following. **P11** has a much higher fluorescence quantum efficiency (Φ_F = 18.0%) than **P12** (Φ_F = 4.5%) (Fig. 5D). This indicates that the photogenerated geminate pairs have a high probability of recombining in **P11**. Consequently, the density of the photogenerated free charges in the **P11**-based photoreceptor is smaller and its S value becomes lower. The S values for the **P11**/MWNTs- and **P12**/MWNTs-based photoreceptors are boosted up to 505.1 and 4545.5 mm^2 mW^{-1} s^{-1}, respectively (Fig. 5D). Both displayed about a 3-fold improvement in photoconduction performance. Since MWNTs behave as an electron acceptor, the existence of MWNTs in the CGM improves the charge generation efficiency through the mechanism of photoinduced charge transfer from PPAs to MWNTs. Meanwhile, the MWNTs offer one-dimensional electron-transport channels. Their conductive networks quickly transport the photogenerated electrons to the surface of the photoreceptor to neutralize the surface charge, thus resulting in enhanced photosensitivity.

The studies on solvatochromism and photoinduced charge transfer provided solid evidence to support the D–A interaction mechanism. But the conclusion that D–A interactions are an absolute factor in promoting the solvating power of polymers towards CNTs cannot be fully validated until the following two issues have been clearly addressed. On the one hand, for the polymers **P1** and **P11**, the pyrene and triphenylamine pendants have different linking modes with the polymer mainchain. Triphenylamine moieties are conjugated with the PPA mainchain through double bonds in **P11**, while in **P1** the pyrene moieties are non-conjugated with the PPA backbone by the separation of saturated and flexible spacers. The differences in solvating power towards CNTs may be at least partially ascribed to the function of the linker. On the other hand, pyrene and triphenylamine are characterized by a planar and arched molecular shape, respectively. Thus the differences in solvating power towards CNTs may also be associated with the possibility that arch-shaped triphenylamine has a better affinity towards the CNTs' surface. To rule out these two possible factors, we designed and synthesized **P15** and **P16**. In these two polymers, fluorene and carbazole are used as counterpart pendants, which are linked with the PPA backbone through both saturated and flexible spacers to eliminate the conjugation effect. Meanwhile, fluorene and carbazole have a similar shape and size, thus the shape effect can be greatly limited. As shown in Fig. 3, the carbazole-functionalized PPA (**P15**) shows much stronger solvating power towards MWNTs than the fluorene-functionalized PPA (**P16**). The D–A interactions have been further confirmed by the clear solvatochromism and enhanced redox activity of the nanohybrids.[55,58] Through appropriate molecular design, this work provides convincing proof for the involvement of the D–A effect in the polymer wrapping process.

Assuredly, in addition to the π–π stacking, van der Waals and electrostatic interactions, the D–A interaction offers a novel strategy for the design and fabrication of macroscopically processable nanohybrids composed of CNTs and polymers. The mechanism is schematically illustrated in Fig. 6. The strategy has been applied to versatile nanohybrids, including the preparation of a nanohybrid of covalently functionalized MWNTs with poly(*N*-vinyl carbazole) (PVK) *via* RAFT polymerization,[68] the facile preparation of PVK and MWNTs solution and conjugated polymer network nanocomposite film,[69] and the *in situ* synthesis of PVK-functionalized SWNTs with enhanced optical limiting properties.[70] More recently, this strategy has been extended to graphene-based hybrid systems.[71–75]

3 Hybrid of functional PPAs/CNTs as template

3.1 Direct attachment of inorganic nanostructures to hybrids of functional PPA/CNTs

It has been demonstrated adequately that PPA chains can wrap onto the surface of CNTs; thus, functional PPAs possess suitable solvating power towards CNTs in various solvents. At the same time, the aromatic pendants of the functional PPA efficiently enhance the solvating power of the functional PPAs through π–π interactions and D–A interactions. The pyrene-functionalized PPAs provide telling examples.[47] Dissection of the fluorescent properties of the **P6**/MWNTs hybrid displays some meaningful details. In THF solution, the fluorescence quantum yield of the **P6**/MWNTs hybrid (Φ_F = 10.0%) is lower than that of **P6** (Φ_F = 11.4%), indicative of emission quenching caused by the electron or energy transfer between MWNTs and the pyrene moieties sticking on the MWNTs.[47] The fluorescence spectrum

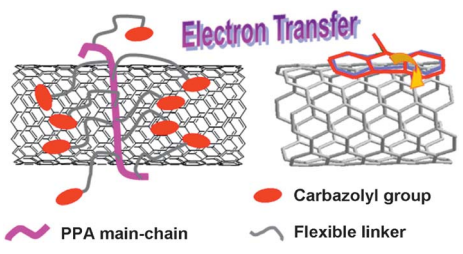

Fig. 6 Illustration of the solvating power of carbazole-functionalized PPA towards CNTs contributed by wrapping of the polymer mainchain, π–π interactions, and donor–acceptor interactions between carbazole pendants and CNTs (right panel). Reproduced with permission from ref. 58. Copyright (2009) Wiley-VCH.

of the hybrids is dominated by the feature of pyrene excimers with an emission maximum at around 480 nm, which indicates the concentration of pyrene moieties in the solution is quite high.

The fluorescence behaviors of **P6**/MWNTs hybrids indicate that the wrapping of PPA chains onto MWNTs simultaneously furnishes the surface of MWNTs with plentiful functional groups. In comparison with the widely used methodology of chemical functionalization of CNTs' surface,[76–80] polymer wrapping is uninjurious to CNTs' structure and properties. Furthermore, the outer functional groups on the wrapping chains can be potentially used to modify the surface chemical properties of CNTs. In this regard, the hybrids of functional PPAs/CNTs can be considered as templates to develop new nanostructures or as building blocks to construct new architectures.

A series of PPA derivatives with different reactive functionalities, such as amino (**P8**) and carboxylic (**P9**), thiol (**P17**, **P18**, **P20–P24**, Chart 4), were synthesized. Thiol is widely used as a capping agent to passivate the surface of II–VI group semiconductor nanostructures, and the surface modification also bestows the nanostructures with desirable solubility in some solvents. Accordingly, thiol-containing PPAs are expected to inherit the binding ability to metal cations including Zn^{2+}, Cd^{2+}, Ag^{+}, *etc.* This was confirmed by experiments on the selective chemical adsorption of ZnO nanoparticles on casting films of thiol-functionalized PPA derivatives.[81] The casting films were dipped perpendicularly into a suspension of ZnO nanoparticles in ethanol for 1 h and then taken out and rinsed with ethanol several times. The surface morphologies of the films before and after ZnO suspension treatment were measured by atomic force microscopy (AFM) in tapping mode and are shown in Fig. 7.

The AFM image of the as-prepared film of **P17** reveals that the film surface is a flat plane with a maximum surface fluctuation of about 28 nm, indicating that the surface of the film is quite smooth. In contrast, after treating with a suspension of ZnO nanoparticles, the surface morphology changed greatly, with particles of 100–200 nm in size spread over the film's surface (Fig. 7B). The maximum fall from the top of the particle to the bottom of the furrow is ~235 nm, much larger than that in Fig. 7A. The particles on the film surface are confirmed to be ZnO nanoparticles by elemental analysis. Comparatively, the AFM image of the PPA film features a smooth plane with fluctuations as small as ~15 nm. After treatment using a ZnO nanoparticle suspension, the film morphology changes little,

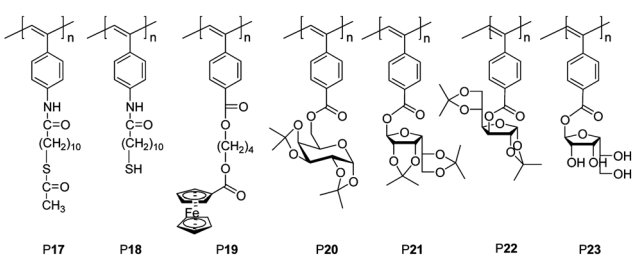

Chart 4 Chemical structures of functional PPAs with functional groups for anchoring inorganic nanostructures and showing the biocompatibility.

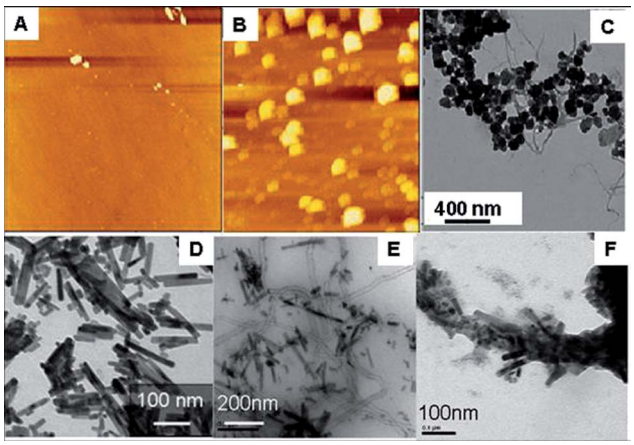

Fig. 7 (A) A typical AFM image of the surface morphology of the pristine casting film of PPA. (B) A typical AFM image showing the scattering of ZnO nanoparticles on the casting film of **P17**. (C) A typical TEM image showing the deposition of ZnO nanoparticles on the surface of MWNTs wrapped by **P17**. TEM images of CdS nanorods (D), dispersion of CdS nanorods and CNTs in PPA matrix (E), and attachment of CdS nanorods along the CNT trunk (F). Adapted with permission from ref. 81. Copyright (2008) American Chemical Society.

with only tiny dots sparsely left on the surface. The interactions between the sulfur atoms of **P17** and the Zn in the nanoparticles are believed to be the driving force for the chemisorption of ZnO nanoparticles onto the surface of **P17** film.

After wrapping onto the CNTs' surface, the interaction between thiols and metal cations stems from the maternal polymers, thus the nanostructures of II–VI semiconductors can chemically adsorb onto the surface of the thiol-functionalized PPA/CNTs hybrids. As shown by Fig. 7C, it seems that the ZnO nanoparticles are attached to the surface of the CNTs.[82] An idea came to us that the inorganic nanostructures can "soft-land" on CNTs with the aid of the functional PPA interlayer. By this strategy, both the inorganic nanostructures and the CNTs can preserve their own structures and properties. This idea was soon validated by the investigation on adhering CdS nanorods to the surface of MWNTs. CdS nanorods were prepared using a solvothermal technique and the typical morphology is shown in

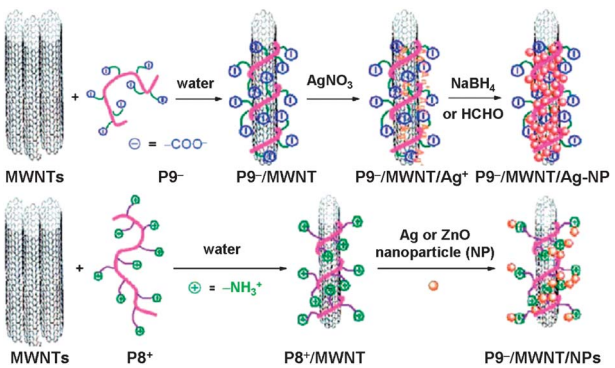

Scheme 1 Illustration of dispersing MWNTs from bundles to single tubes by the wrapping of polymer chains (**P8**$^{+}$ and **P9**$^{-}$) and subsequent deposition of Ag or ZnO nanostructures on the surface of the polymer/MWNTs hybrids. Reproduced with permission from ref. 53. Copyright (2009) American Chemical Society.

Fig. 7D. Simply mixing CdS nanorods with MWNTs gave rise to an isolated and messy arrangement of the two components (Fig. 7E). After wrapping **P18** polymer chains on the MWNTs' surface, CdS nanorods lean closely to the MWNTs, just like aerophytes twisting around a trunk (Fig. 7F).

3.2 Growing inorganic nanostructures on the surface of CNTs by chemical reactions of functional PPA/CNTs hybrids

As illustrated in Scheme 1, the bundles of MWNTs are dispersed in solvent by **P9**. The wrapping of PPA mainchains on MWNTs achieves surface functionalization of MWNTs with carboxylic or amino groups. Considering that carboxylic groups can coordinate with different metal cations, the obtained hybrid of **P9**$^{-}$/MWNTs is a desirable candidate for carriers of metal cations. Ag^{+} was firstly tried in our investigations and silver nanoparticles were expected to be deposited on the MWNT surface by the reduction of the Ag^{+} cations with appropriate reducing agents. As displayed by the TEM and SEM images shown in Fig. 8A and B, by *in situ* reduction with $NaBH_4$, the Ag^{+} cations are transformed to Ag nanoparticles with diameters of ~10–50 nm that are densely bound to the MWNT walls. The spot circled in Fig. 8A has been analyzed by energy-dispersive X-ray (EDX) spectroscopy and was confirmed to be silver nanoparticles (Fig. 8D). The formation of Ag nano-particles was also confirmed by the sharp plasmonic absorption recorded for the resulting hybrid of Ag@**P9**/MWNTs.[83]

When formaldehyde was used as a reductant, the morphologies of the resultant hybrids changed remarkably. A thin film with silver nanoparticles embedded in the coating matrices (Fig. 8C), rather than nanoparticles is formed. The formation of these unique morphologies is understandable. The reduction of Ag^{+} by formaldehyde under mild conditions is a classic silver mirror reaction; in the presence of MWNTs, the silver mirror naturally forms and overcoats on the tube surface.

Not only the reduction of metal cations to metal nanoparticles, but also the oxidation of metal containing organic precursors to nanoscale metal oxides can be realized through polymer/CNTs hybrids. It has been demonstrated that ferrocene-containing PPAs are suitable for dispersing CNTs in organic solvents. Thus, highly processable ferrocene-functionalized PPAs/CNTs hybrids have been prepared.[54] Ceramic products are derived from **P19** and **P19**/MWNT hybrid under carbonization in argon atmosphere at 1000 °C for 1 h and the ceramic yields for **P19** and **P19**/MWNTs are 30.9% and 44.3%, respectively. SEM images clearly show the presence of MWNTs in the ceramic products from **P19**/MWNTs because MWNTs are stable at 1000 °C. Both of the resulting powders can be attracted to a bar magnet, indicating the existence of γ-Fe_2O_3. X-Ray diffraction patterns for the ceramics obtained from pure **P19** and **P19**/MWNTs hybrid are assigned to γ-Fe_2O_3, in comparison with the pattern of the γ-Fe_2O_3 standard. The existence of the Fe element in both samples was further confirmed by X-ray photoelectron spectroscopy (XPS) and energy-dispersive X-ray (EDX) analyses.[54] The magnetization measurements on a Quantum Design vibrating sample magneto-meter at room temperature revealed that both pure **P19** and **P19**/MWNTs hybrid gave rise to superparamagnetic ceramics, and the corresponding saturation magnetizations (M_s) are 29.9 and 26.9 emu g^{-1} (Fig. 9). The data are in the list of the best results reported for magnetic nanocomposites obtained at that time by the attachment of magnetic nanoparticles onto CNTs.[84]

4 Biomaterials based on hybrids of functional PPAs/CNTs

CNTs are deemed to be the toughest nanomaterial and are widely used as additives to reinforce polymer materials.[85] Appropriately surface modified CNTs have shown to be biocompatible and to be potentially applied in the areas of tissue engineering and drug delivery systems.[80,86–90] Meanwhile, a recent investigation of the response of bone cells to MWNTs indicated that MWNTs inhibit osteoclastic bone resorption *in vivo* and suppressed a transcription factor essential for

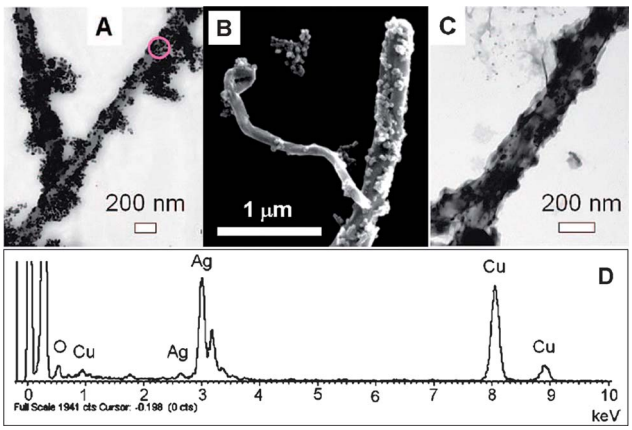

Fig. 8 (A) and (C) show typical TEM images of MWNTs decorated with silver nanoparticles and silver coating, respectively. (B) Displays a typical SEM image of MWNTs decorated with silver nanoparticles. (D) presents the energy-dispersive X-ray (EDX) spectrum for the spot circled in (A). Adapted with permission from ref. 53. Copyright (2009) American Chemical Society.

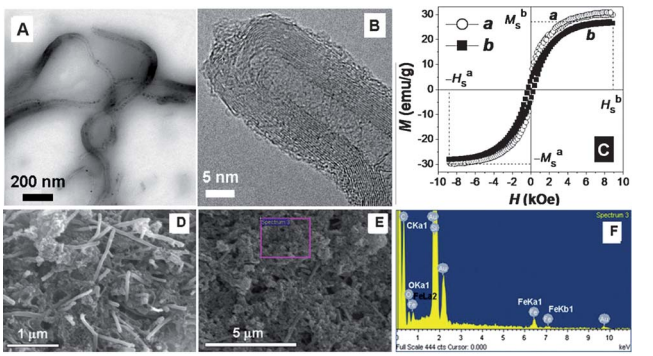

Fig. 9 (A) and (B) are typical TEM and high resolution TEM images of **P19**/MWNT, respectively. (C) Magnetization curves for the ceramic products obtained from (a) **P19** and (b) **P19**/MWNT hybrid at room temperature. (D and E) SEM graphs of ceramic products obtained from **P19** and **P19**/MWNT hybrid under argon at 1000 °C for 1 h, respectively. (F) EDX spectrum of ceramic products from **P19**/MWNT hybrid. Reproduced with permission from ref. 54. Copyright (2008) American Chemical Society.

osteoclastogenesis *in vitro*.[91,92] These results suggest that MWNTs have beneficial effects on bone growth. Therefore, it is rational to use MWNTs for the reinforcement of chitosan (CS) rods because the bending strength and modulus of the pure CS rods made by *in situ* precipitation are lower than the quota for internal fixation of bone fracture in clinical application.[93,94]

To get the advantages of MWNTs for the reinforcement of CS rods, the premise of uniformly dispersing MWNTs in aqueous media has to be met. The hybrid of **P8**$^+$/MWNTs is an opportune candidate. Coincidentally, the fabrication of CS rods by an *in situ* precipitation method is conducted in acidic aqueous solution, which is also suitable for dissolving the hybrid of **P8**$^+$/MWNTs. It is expected that the bending strength and modulus can be enhanced when the MWNTs are aligned parallel to the axial direction of a CS rod. According to the literature, the alignment of MWNTs could be induced by using magnetic force when magnetic nanoparticles are deposited on the surface of MWNTs.[95] The strategy described in Section 3.1 finds its application in this case. The magnetic Fe_3O_4 nanoparticles were chemically deposited onto the surface of the **P8**$^+$/MWNTs hybrid by the coordination of amino groups to Fe^{2+} and Fe^{3+} cations. The acidic solution containing MWNTs decorated with Fe_3O_4 nanoparticles and **P8**$^+$ polycations was mixed with CS solution. The mixture was filled into a cylindrical mold, which was immersed into a basic solution for *in situ* precipitation. During the precipitation process, an external magnetic field was applied in the axial direction of the cylindrical mold.

As shown in Scheme 2, upon the inducement of the external magnetic field, the Fe_3O_4@**P8**$^+$/MWNTs nanostructures gradually aligned in the axial direction of the cylindrical mold. The average bending strength and bending modulus of the finally produced reinforced CS rods are 124.6 MPa and 5.3 GPa,

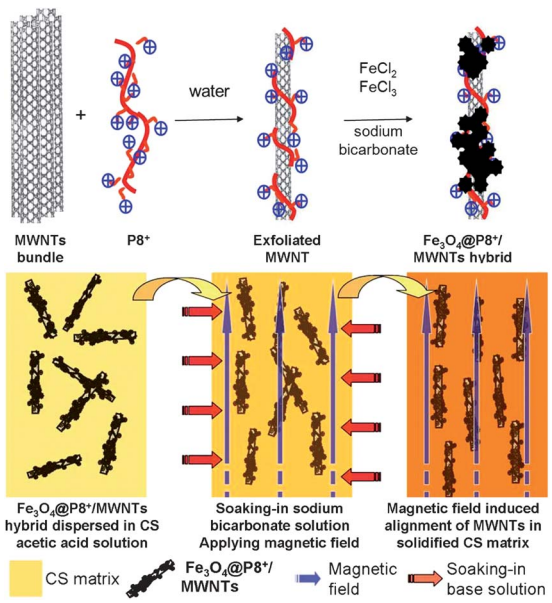

Scheme 2 Synthetic route to the triple-component hybrid of Fe_3O_4@**P8**$^+$/MWNT and a schematic illustration of the magnetic-field-induced alignment of the hybrids in the CS matrix. Reproduced with permission from ref. 60. Copyright (2011) Elsevier.

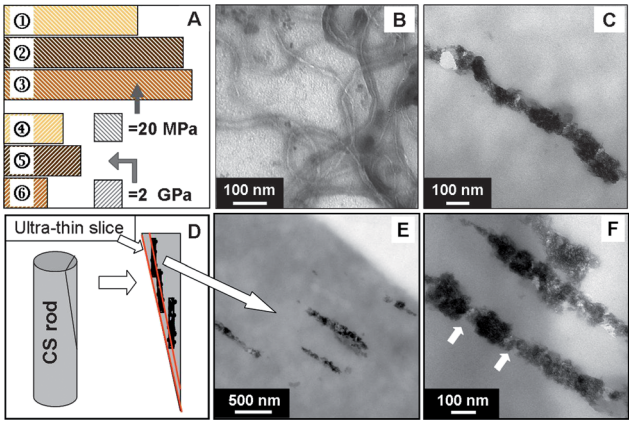

Fig. 10 (A) Quantitative comparison of the bending strength (①: pure CS rod, ②: CS rod reinforced with Fe_3O_4@**P8**$^+$/MWNTs hybrid, ③: Dikfix, commercially available product) and bending modulus (④: pure CS rod ⑤: CS rod reinforced with Fe_3O_4@**P8**$^+$/MWNTs hybrid, ⑥: Dikfix). (B) and (C) are respectively the TEM images of **P8**$^+$/MWNTs hybrids and Fe_3O_4@**P8**$^+$/MWNTs. (C) An illustration of cutting the ultra-thin slices; (D) a typical TEM image of the ultra-thin slice from a CS rod reinforced with Fe_3O_4@**P8**$^+$/MWNTs hybrid; (C) a magnified image showing the existence of pure MWNTs (arrows). Adapted with permission from ref. 60. Copyright (2011) Elsevier.

respectively, which are 34.8% and 29.3% higher than the pure CS rods. These data indicate that the key mechanical properties of the CS rods reinforced with axially aligned MWNTs are approximate to the commercially available product Dikfix. The coating of a polymer layer and the successive growth of Fe_3O_4 on the surface of MWNTs were shown by the TEM images in Fig. 10B and C, respectively. The alignment of the MWNTs in the CS matrix is confirmed by the TEM images given in Fig. 10E and F, which demonstrates that several rod-like nano-sized entities assigned to the Fe_3O_4@**P8**$^+$/MWCNTs can be observed. The ultra-thin slices were prepared as illustrated in Fig. 10D. The existence of magnetic Fe_3O_4@**P8**$^+$/MWNTs nanohybrids in the prepared composite CS rods was also confirmed by SEM images, X-ray diffraction (XRD) patterns and magnetization measurements.

Although **P8** and **P9** are respectively soluble in acidic and basic aqueous solutions, they cannot be used directly in biological situations due to the harsh acid and base conditions. Some PPA derivatives bearing biomolecular functionalities such as monosaccharides and nucleotides are biocompatible and harmless to cells.[96,97] In addition, they are directly soluble in water and different buffer solutions that have been widely used in biological investigations. Meanwhile, it has been demonstrated that polymers and oligomers containing saccharide moieties can be utilized to disperse CNTs in aqueous solutions.[98–101] If monosaccharides are properly linked to the PPA mainchain, the saccharide pendants and the PPA backbone may play the roles of improving the biocompatibility and wrapping and dispersing MWNTs in aqueous media, respectively. Therefore, a series of PPA derivative bearing monosaccharides (D-glucose, D-mannose and D-galactose) were synthesized (Chart 4, **P20**, **P21** and **P22**) and used to try to disperse MWNTs in water.

However, the primary experimental results were disappointing. All of the monosaccharide-functionalized PPAs

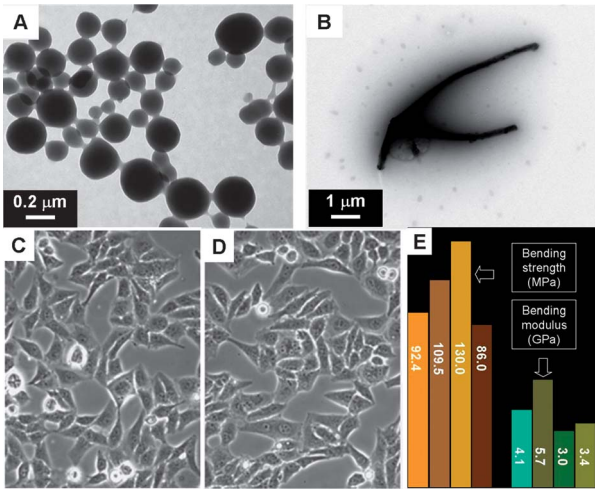

Fig. 11 (A) and (B) are TEM images of **P21** being precipitated in methanol and the counterpart of *in situ* polymerization in the presence of MWNTs in THF, respectively. (C) and (D) Adhesion of living HeLa cells to the microtiter plates precoated with **P21**/MWNTs (0.05 mg mL^{-1}) and the control (D), respectively. (E) Quantitative description of the bending strength and bending modulus (from left to right, pure CS rod, CS rod reinforced with **P23**/MWNTs nanohybrid, Dikfix, CS rod reinforced with the addition of 5% hydroxyapatite).

showed very limited solvating power towards MWNTs in water despite the good water-solubility of the polymers themselves. We recognized that the saccharide pendants can induce the formation of mainchain helicity and can simultaneously encircle the mainchain, which greatly decreases the ability of the PPA mainchain to wrap MWNTs. Rationally, we turned to *in situ* polymerization of saccharide-modified phenylene monomers in the presence of pretreated MWNTs, and the results were satisfactory. For example, the solubility of **P21**/MWNTs hybrid is about 170 mg L^{-1} in DMF (dimethylformamide) solvent. As revealed by the TEM images, without MWNTs, **P21** polymer chains have a spherical micro-morphology (Fig. 11A), but cling to MWNTs in the hybrid (Fig. 11B). The films of the **P21**/MWNTs hybrid casting on microtiter plates allow for normal adhesion and growth of HeLa cells after incubation for 1 day in comparison with a control sample (Fig. 11C and D), indicating the good biocompatibility of the **P21**/MWNTs hybrid.

The **P21**/MWNTs hybrid was also tried to be used for the reinforcement of CS rods. Before introducing the hybrid into CS solution, the hydroxylics in **P21** had to be deprotected in order to recover the biological activity of the sugar and enhance the compatibility with the CS component (Chart 4, **P23**). When about 3% (by weight) **P23**/MWNTs was introduced into the CS solution, the average bending strength and bending modulus of the obtained composite CS rods are 109.5 MPa and 5.7 GPa, respectively. These values are 18.5% and 28.1% higher than the pure CS rods, and 27.3% and 67.6% higher than the pure CS rods composed of 5% (by weight) hydroxyapatite (Fig. 11E).

5 Conclusions and outlook

The hybrids of functional PAs/CNTs have shown attractive properties. By integrating the factors of wrapping with polymer mainchain, π–π and/or D–A interactions between aromatic pendants and CNTs, and the flexible linker between the pendant and mainchain, functional PPAs demonstrate strong solvating power towards CNTs in different solvents, including water. Specially designed functional PPAs are in the list of most powerful dispersants of CNTs among all organic and polymeric materials. In particular, the discrimination of D–A interactions out of popularly accepted π–π interactions provides a distinct factor to project novel functional polymers for dispersing CNTs in different matrices. However, there is still space for accommodating new measures to strengthen the solvating power and to exert unique functions. In view of the structure parameters, the induced helicity of the PPA mainchain has not been integrated into the factors for solvating CNTs. Combining the helicity with D–A interactions, novel functional PPAs may find application in the separation of CNTs with different electronic structures and/or with different diameters. This strategy was primarily demonstrated by Wenzel and colleagues. They found that poly(*N*-decyl-2,7-carbazole) exclusively dispersed semiconducting SWNTs with differences of their chiral indices $(n–m) \geq 2$ in toluene; while the fluorene analogue poly(9,9-dialkyl-2,7-fluorene) selectively dispersed semiconducting SWNTs with $(n–m) \leq 2$ in toluene.[102]

Graphene, as an allotrope of CNTs has attracted considerable research interest because of its unique structure and properties. It is of fundamental importance to effectively exfoliate single-layered and few-layered graphenes from graphite and to stabilize the exfoliated graphenes in solvents. In the past decade, many organic and polymeric agents have been tried and a few methodologies have been established. In this aspect, few attempts have been carried out to use functional PAs as dispersing agents.[71,74] Considering the remarkable difference in their shapes, wrapping graphene with PA mainchains is an inaccessible approach, but the fused cyclic aromatic pendants and shape-persistent conjugated mainchains are thought to have positive effects. In addition, graphene can be considered as a platform on which the polymerization of functional acetylenes can be initiated. This strategy was successfully adopted for the fabrication of the hybrids of PPA and C60 by Tang and coworkers.[105]

The effective reinforcement of CS rods displays promising application as bioconjugate materials for the hybrids of functional PPAs/MWNTs. Certainly, a more reasonable polymer design, more detailed investigations on the conditions for composite fabrication, longer term stability of the hybrids and more biochemical and biophysical assays should be performed before they are pushed into clinical practice. In this review, we pay more attention to the functional PAs. This is only one component of the hybrid. In fact, the intrinsic properties of CNTs such as their high electronic conductivity, high charge transportability, and high environment stability should be always kept in mind. These properties of CNTs provide a unique opportunity for the direct electron transfer between the biological and chemical analytes in the active electrode area.[80b,c] It has been confirmed that CNTs have excellent electrocatalytic activities for the redox reaction of hydrogen peroxide and nicotinamide adenine dinucleotide, two major by-products of

enzymatic reactions, which indicate a promising future for the simple design and implementation of on-site biosensors for oxidases and dehydrogenases with enhanced selectivity.[103,104] The development of biomolecule-functionalized and water-soluble PPAs offers a chance for to explore the applications of the hybrids in chemo- and biosensors. In this regard, the intrinsic properties of CNTs and multiple surface functionalizations will exhibit the advantages of high sensitivity, improved selectivity and device miniaturization.

Acknowledgements

This work is supported by the National Science Foundation of China (21074113 and 20974028), the Ministry of Science and Technology of China (2009CB623605), the Research Grants Council of Hong Kong (603509, HKUST2/CRF/10, and 604711), the SRFI grant of HKUST (SRFI11SC03PG), the NSFC/RGC grant (N_HKUST620/11), the University Grants Committee of Hong Kong (AoE/P-03/08). B.Z.T. thanks the Cao Guangbiao Foundation of Zhejiang University for the support.

Notes and references

1 A. J. Heeger, *Rev. Mod. Phys.*, 2001, **73**, 681–718.
2 H. Shirakawa, *Angew. Chem., Int. Ed.*, 2001, **40**, 2575–2580.
3 A. G. MacDiarmid, *Angew. Chem., Int. Ed.*, 2001, **40**, 2581–2590.
4 A. J. Heeger, *Chem. Soc. Rev.*, 2010, **39**, 2354–2371.
5 W. Y. Lam, X. Kong and B. Z. Tang, *Macromolecules*, 2000, **33**, 5027–5040; S.-Y. Oh, K. Akagi, H. Shirakawa and K. Araya, *Macromolecules*, 1993, **26**, 6203–6206.
6 W. Y. Lam, Y. Dong, H. S. Kwok, J. C. Shen and B. Z. Tang, *Macromolecules*, 2005, **38**, 3290–3300.
7 C. Ye, W. Y. Lam, Z.-F. Liu, S. Z. D. Cheng, E.-Q. Chen and B. Z. Tang, *J. Am. Chem. Soc.*, 2005, **127**, 7668–7669.
8 R. Sun, T. Masuda and T. Kobayashi, *Synth. Met.*, 1997, **91**, 301–303.
9 Y. Wang, R. Sun, D. Wang, T. M. Swager and A. J. Epstein, *Appl. Phys. Lett.*, 1999, **74**, 2593–2595.
10 R. Hidayat, A. Fujii, M. Ozaki, M. Teraguchi, T. Masuda and K. Yoshino, *Synth. Met.*, 2001, **119**, 597–598.
11 Y. Huang, W. Y. Lam and B. Z. Tang, *Appl. Phys. Lett.*, 2001, **78**, 1652–1654.
12 W. Z. Yuan, A. J. Qin, J. W. Y. Lam, J. Z. Sun, Y. Q. Dong, J. Z. Liu, H. P. Xu, Q. Zheng and B. Z. Tang, *Macromolecules*, 2007, **40**, 3159–3166.
13 A. Qin, C. K. W. Jim, Y. Tang, J. W. Y. Lam, J. Liu, M. Faisal, P. Gao and B. Z. Tang, *J. Phys. Chem. B*, 2008, **112**, 9281–9288.
14 B. Z. Tang and N. Kotera, *Macromolecules*, 1989, **22**, 4388–4392.
15 B. Z. Tang, H. Peng and H. N. C. Wong, *Chin. J. Polym. Sci.*, 1999, **17**, 81–86.
16 V. Percec, E. Aqad, M. Peterca, J. G. Rudick, L. Lemon, J. C. Ronda, B. B. De, P. A. Heiney and E. W. Meijer, *J. Am. Chem. Soc.*, 2006, **128**, 16365–16372.
17 K. Akagi, G. Piao, S. Kaneko, K. Sakamaki, H. Shirakawa and M. Kyotani, *Science*, 1998, **282**, 1683–1686.
18 K. Akagi, *J. Polym. Sci., Part A: Polym. Chem.*, 2009, **47**, 2463–2485.
19 K. Akagi, S. Guo, T. Mori, M. Goh, G. Piao and M. Kyotani, *J. Am. Chem. Soc.*, 2005, **127**, 14647–14654.
20 K. Nagai, T. Masuda, T. Nakagawa, B. D. Freeman and Z. Pinnau, *Prog. Polym. Sci.*, 2001, **26**, 721–798.
21 T. Masuda, *J. Polym. Sci., Part A: Polym. Chem.*, 2007, **45**, 165–180.
22 W. Y. Lam and B. Z. Tang, *J. Polym. Sci., Part A: Polym. Chem.*, 2003, **41**, 2607–2629.
23 W. Y. Lam and B. Z. Tang, *Acc. Chem. Res.*, 2005, **38**, 745–754.
24 J. Z. Liu, W. Y. Lam and B. Z. Tang, *Chem. Rev.*, 2009, **109**, 5799–5867.
25 K. Akagi, *Chem. Rev.*, 2009, **109**, 5354–5401.
26 M. Goh, S. Matsushita and K. Akagi, *Chem. Soc. Rev.*, 2010, **39**, 2466–2476.
27 B. M. Rosen, C. J. Wilson, D. A. Wilson, M. Peterca, M. R. Imam and V. Percec, *Chem. Rev.*, 2009, **109**, 6275–6540.
28 Y. W. Park, *Chem. Soc. Rev.*, 2010, **39**, 2428–2438.
29 E. Yashima, K. Maeda and Y. Furusho, *Acc. Chem. Res.*, 2008, **41**, 1166–1180.
30 E. Yashima, K. Maeda, H. Iida, Y. Furusho and K. Nagai, *Chem. Rev.*, 2009, **109**, 6102–6211.
31 S. Srivastava and N. A. Kotov, *Acc. Chem. Res.*, 2008, **41**, 1831–1841.
32 N. Tomczak, D. Janczewski, M. Han and G. J Vancso, *Prog. Polym. Sci.*, 2009, **34**, 393–430.
33 G. V. Ramesh, S. Porel and T. P. Radhakrishnan, *Chem. Soc. Rev.*, 2009, **38**, 2646–2656.
34 Y. Park and R. C. Advincula, *Chem. Mater.*, 2011, **23**, 4273–4294.
35 K. Haraguchi, *Polym. J.*, 2011, **43**, 223–241.
36 O. Matarredona, H. Rhoads, Z. R. Li, J. H. Harwell, L. Balzano and D. E. Resasco, *J. Phys. Chem. B*, 2003, **107**, 13357–13367.
37 K. Yurekli, C. A. Mitchell and R. Krishnamoorti, *J. Am. Chem. Soc.*, 2004, **126**, 9902–9903.
38 B. I. Kharisov, O. V. Kharissova, H. L. Gutierrez and U. O. Mendez, *Ind. Eng. Chem. Res.*, 2009, **48**, 572–590.
39 B. Z. Tang and H. Xu, *Macromolecules*, 1999, **32**, 2569–2576.
40 Z. Li, Y. Q. Dong, M. Häußler, J. W. Y. Lam, Y. P. Dong, L. Wu, K. S. Wong and B. Z. Tang, *J. Phys. Chem. B*, 2006, **110**, 2302–2309.
41 D. M. Guldi, G. M. A. Rahman, F. Zerbetto and M. Prato, *Acc. Chem. Res.*, 2005, **38**, 871–878.
42 D. M. Guldi, G. M. A. Rahman, N. Jux, D. Balbinot, U. Hartnagel, N. Tagmatarchis and M. Prato, *J. Am. Chem. Soc.*, 2005, **127**, 9830–9838.
43 C. Ehli, G. M. A. Rahman, N. Jux, D. Balbinot, D. M. Guldi, F. Paulucci, M. Marcaccio, D. Paolucci, M. Melle-Franco, F. Zerbetto, S. Campidelli and M. Prato, *J. Am. Chem. Soc.*, 2006, **128**, 11222–11231.

44 Y. Zhang, S. Yuan, W. Zhou, J. Xu and Y. Li, *J. Nanosci. Nanotechnol.*, 2007, **7**, 2366–2375.
45 G. J. Bahun, C. Wang and A. Adronov, *J. Polym. Sci., Part A: Polym. Chem.*, 2006, **44**, 1941–1951.
46 W. Z. Yuan, J. Z. Sun, Y. Q. Dong, M. Häußler, F. Yang, H. P. Xu, A. Qin, J. W. Y. Lam, Q. Zheng and B. Z. Tang, *Macromolecules*, 2006, **39**, 8011–8020.
47 W. Z. Yuan, Y. Mao, H. Zhao, J. Z. Sun, H. P. Xu, J. K. Jin, Q. Zheng and B. Z. Tang, *Macromolecules*, 2008, **41**, 701–707.
48 H. Shirakawa, E. Louis, A. G. MacDiarmid, C. K. Chiang and A. J. Heeger, *J. Chem. Soc., Chem. Commun.*, 1977, 578–580.
49 Y. Tanabe, H. Kyotani, K. Akagi and H. Shirakawa, *Macromolecules*, 1995, **28**, 4173–4178.
50 B. Z. Tang, X. Kong, X. Wan and X.-D. Feng, *Macromolecules*, 1997, **30**, 5620–5628.
51 J. Z. Sun, H. Z. Chen, R. S. Xu, M. Wang, J. W. Y. Lam and B. Z. Tang, *Chem. Commun.*, 2002, 1222–1223.
52 J. W. Y. Lam and B. Z. Tang, *J. Polym. Sci., Part A: Polym. Chem.*, 2003, **41**, 2607–2629.
53 W. Z. Yuan, L. Tang, H. Zhao, J. K. Jin, J. Z. Sun, A. Qin, H. P. Xu, J. Liu, F. Yang, Q. Zheng, E. Chen and B. Z. Tang, *Macromolecules*, 2009, **42**, 52–61.
54 W. Z. Yuan, J. Z. Sun, J. Z. Liu, Y. Q. Dong, Z. Li, H. P. Xu, A. Qin, M. Haeussler, J. K. Jin, Q. Zheng and B. Z. Tang, *J. Phys. Chem. B*, 2008, **112**, 8896–8905.
55 H. Zhao, W. Z. Yuan, L. Tang, J. Z. Sun, H. P. Xu, A. Qin, Y. Mao, J. K. Jin and B. Z. Tang, *Macromolecules*, 2008, **41**, 8566–8574.
56 J. Wang, H. Zhao, C. G. Cai, Y. Mao, L. Tang, X. Y. Shen, H. P. Xu, W. Z. Yuan, J. Z. Sun and B. Z. Tang, *Acta Polym. Sin.*, 2009, **52**, 293–297.
57 W. Z. Yuan, J. W. Y. Lam, X. Y. Shen, J. Z. Sun, F. Mahtab, Q. Zheng and B. Z. Tang, *Macromolecules*, 2009, **42**, 2523–2531.
58 H. Zhao, W. Z. Yuan, J. Mei, L. Tang, X. Q. Liu, J. M. Yan, X. Y. Shen, J. Z. Sun, A. Qin and B. Z. Tang, *J. Polym. Sci., Part A: Polym. Chem.*, 2009, **47**, 4995–5005.
59 W. Z. Yuan, H. Zhao, X. Y. Shen, F. Mahtab, J. W. Y. Lam, J. Z. Sun and B. Z. Tang, *Macromolecules*, 2009, **42**, 9400–9411.
60 Z. Wang, H. Zhao, L. Fan, J. Lin, P. Zhuang, W. Z. Yuan, Q. Hu, J. Z. Sun and B. Z. Tang, *Carbohydr. Polym.*, 2011, **84**, 1126–1132.
61 X. A. Zhang, A. Qin, L. Tong, H. Zhao, Q. Zhao, J. Z. Sun and B. Z. Tang, *Macromolecules*, 2011, **44**, 6724–6737.
62 X. A. Zhang, H. Zhao, Y. Gao, J. Tong, L. Shan, Y. Chen, S. Zhang, J. Z. Sun, A. Qin and B. Z. Tang, *Polymer*, 2011, **52**, 5290–5301.
63 L. Tong, A. Qin, X. A. Zhang, Y. Mao, J. Z. Sun and B. Z. Tang, *Sci. China: Chem.*, 2011, **12**, 1948–1954.
64 W. Z. Yuan, H. Zhao, H. P. Xu, J. Z. Sun, J. W. Y. Lam, Y. Mao, J. K. Jin, S. Zhang, Q. Zheng and B. Z. Tang, *Acta Polym. Sin.*, 2007, **50**, 901–904.
65 B. Z. Tang, H. Chen, R. Xu, J. W. Y. Lam, K. K. L. Cheuk, H. N. C. Wong and M. Wang, *Chem. Mater.*, 2000, **12**, 213–221.
66 H. Xu, J. Sun, A. Qin, J. Hua, Z. Li, Y. Q. Dong, H. Xu, W. Yuan, Y. Ma, M. Wang and B. Z. Tang, *J. Phys. Chem. B*, 2006, **110**, 21701–21709.
67 H. P. Xu, B. Y. Xie, W. Z. Yuan, J. Z. Sun, F. Yang, Y. Q. Dong, A. Qin, S. Zhang, M. Wang and B. Z. Tang, *Chem. Commun.*, 2007, 1322–1324.
68 B. Zhang, J. Wang, Y. Chen, D. FruCht, B. Yu, X. Zhuang, N. He and W. J. Blau, *J. Polym. Sci., Part A: Polym. Chem.*, 2010, **48**, 3161–3168.
69 K. M. Cui, M. C. Tria, R. Pernites, C. A. Binag and R. C. Advincula, *ACS Appl. Mater. Interfaces*, 2011, **3**, 2300–2308.
70 P. Li, L. Niu, Y. Chen, J. Wang, Y. Liu, J. Zhang and W. J. Blau, *Nanotechnology*, 2011, **22**, 015204.
71 D.-E. Jiang, X.-Q. Chen, W. D. Luo and W. A. Shelton, *Chem. Phys. Lett.*, 2009, **483**, 120–123.
72 J. Liu, W. Yang, L. Tao, D. Li, C. Boyer and T. P. Davis, *J. Polym. Sci., Part A: Polym. Chem.*, 2010, **48**, 425–433.
73 M. K. Singh, E. Titus, G. Goncalves, P. A. A. P. Marques, I. Bdikin, A. L. Kholkin and J. J. A. Gracio, *Nanoscale*, 2010, **2**, 700–708.
74 X. Xu, Q. Luo, W. Lv, Y. Q. Dong, Y. Lin, Q. Yang, A. Shen, D. Pang, J. Hu, J. G. Qin and Z. Li, *Macromol. Chem. Phys.*, 2011, **212**, 768–773.
75 A. B. Kaiser and V. Skakalova, *Chem. Soc. Rev.*, 2011, **40**, 3786–3801.
76 Please see special issue of *Acc. Chem. Res.*, 2002, **35**(12): (*a*) R. Andrews, D. Jacques, D. Qian and T. Rantell, *Acc. Chem. Res.*, 2002, **35**, 1008–1017; (*b*) M. Ouyang, J.-L. Huang and C. M. Lieber, *Acc. Chem. Res.*, 2002, **35**, 1018–1025; (*c*) P. Avouris, *Acc. Chem. Res.*, 2002, **35**, 1026–1034; (*d*) H. Dai, *Acc. Chem. Res.*, 2002, **35**, 1035–1044; (*e*) Y.-P. Sun, K. Fu, Y. Lin and W. Huang, *Acc. Chem. Res.*, 2002, **35**, 1096–1104.
77 A. Hirsch, *Angew. Chem., Int. Ed.*, 2002, **41**, 1853–1859.
78 H. Kong, C. Gao and D. Yan, *J. Am. Chem. Soc.*, 2004, **126**, 412–413.
79 S. Srivastava and N. A. Kotov, *Acc. Chem. Res.*, 2008, **41**, 1831–1841.
80 Recent reviews: (*a*) B. Li and W.-H. Zhong, *J. Mater. Sci.*, 2011, **46**, 5595–5614; (*b*) S. K. Vashist, D. Zheng, K. Al-Rubeaan, J. H. T. Luong and F.-S. Sheu, *Biotechnol. Adv.*, 2011, **29**, 169–188; (*c*) M. van der Zande, R. Junker, X. F. Walboomers and J. A. Jansen, *Tissue Eng., Part B: Rev.*, 2011, **17**, 57–69; (*d*) X. H. Peng and S. S. Wong, *Adv. Mater.*, 2009, **21**, 625–642.
81 H. P. Xu, J. K. Jin, Y. Mao, J. Z. Sun, F. Yang, W. Z. Yuan, Y. Q. Dong, M. Wang and B. Z. Tang, *Macromolecules*, 2008, **41**, 3874–3883.
82 H. P. Xu, Y. Mao, W. Z. Yuan, J. Z. Sun, Y. Q. Dong, M. Wang and B. Z. Tang, *Acta Polym. Sin.*, 2007, **50**, 897–900.
83 S. Magdassi, A. Bassa, Y. Vinetsky and A. Kamyshny, *Chem. Mater.*, 2003, **15**, 2208–2217.

84 Representative examples: (*a*) J. Wan, W. Cai, J. Feng, X. Meng and E. Liu, *J. Mater. Chem.*, 2007, **17**, 1188–1192; (*b*) K. Kordas, T. Mustonen, G. Toth, J. Vahakangas, A. Uusimaki, H. Jantunen, A. Gupta, K. V. Rao, R. Vajtai and P. M. Ajayan, *Chem. Mater.*, 2007, **19**, 787–791; (*c*) V. Georgakilas, V. Tzitzios, D. Gournis and D. Petridis, *Chem. Mater.*, 2005, **17**, 1613–1617.

85 M. S. Dresselhaus, G. Dresselhaus and P. C. Eklund, *Science of Fullerenes Carbon Nanotubes*, Academic Press, San Diego, 1996.

86 N. Saito, Y. Usui, K. Aoki, N. Narita, M. Shimizu, K. Hara, N. Ogiwara, K. Nakamura, N. Ishigaki, H. Kato, S. Taruta and M. Endo, *Chem. Soc. Rev.*, 2009, **38**, 1897–1903.

87 S. Sirivisoot and T. J. Webster, *Nanotechnology*, 2008, **19**, 295101.

88 J. V. Veetil and K. M. Ye, *Biotechnol. Prog.*, 2009, **25**, 709–721.

89 S. M. Hussain, L. K. Braydich-Stolle, A. M. Schrand, R. C. Murdock, K. O. Yu, D. M. Mattie, J. J. Schloger and M. Terrones, *Adv. Mater.*, 2009, **21**, 1549–1559.

90 A. E. Nel, L. Madler, D. Velegol, T. Xia, E. M. V. Hoek and P. Somasundaran, *et al.*, *Nat. Mater.*, 2009, **8**, 543–557.

91 J. L. Xu, K. A. Khor, J. J. Sui and W. N. Chen, *Mater. Sci. Eng., C*, 2009, **29**, 44–49.

92 N. Narita, Y. Kobayashi, H. Nakamura, K. Maeda, A. Ishihara, T. Mizoguchi, Y. Usui, K. Aoki, M. Simizu, H. Kato, N. Udagawa, M. Endo, N. Takahashi and N. Saito, *Nano Lett.*, 2009, **9**, 1406–1412.

93 Q. L. Hu, X. Z. Qian, B. Q. Li and J. C. Shen, *Chem. J. Chin. Univ.*, 2003, **24**, 528–531.

94 Q. L. Hu, B. Q. Li, M. Wang and J. C. Shen, *Biomaterials*, 2004, **25**, 779–785.

95 J. Tumpane, N. Karousis, N. Tagmatarchis and B. Norden, *Angew. Chem., Int. Ed.*, 2008, **47**, 5148–5152.

96 K. K. L. Cheuk, J. W. Y. Lam, B. S. Li, Y. Xie and B. Z. Tang, *Macromolecules*, 2007, **40**, 2633–2642.

97 K. K. L. Cheuk, B. S. Li, J. W. Y. Lam, Y. Xie and B. Z. Tang, *Macromolecules*, 2008, **41**, 5997–6005.

98 J. Chen, M. J. Dyer and M. F. Yu, *J. Am. Chem. Soc.*, 2001, **123**, 6201–6202.

99 J. Lin, C. He, L. Zhang and S. Zhang, *Anal. Biochem.*, 2009, **384**, 130–135.

100 J. Lin, C. He, Y. Zhao, L. Zhang and S. Zhang, *Sens. Actuators, B*, 2009, **137**, 768–773.

101 Z. Zhang, Y. Hu, H. Zhang and S. Yao, *J. Colloid Interface Sci.*, 2010, **344**, 158–164.

102 F. A. Lemasson, T. Strunk, P. Gerstel, F. Hennrich, S. Lebedkn, C. Barner-Kowollik, W. Wenzel, M. M. Kappes and M. Mayor, *J. Am. Chem. Soc.*, 2011, **133**, 652–655.

103 B. Sljukic, C. E. Banks and R. G. Compton, *Nano Lett.*, 2006, **6**, 1556–1558.

104 L. Meng, J. Jin, G. X. Yang, T. H. Lu, H. Zhang and C. X. Cai, *Anal. Chem.*, 2009, **81**, 7271–7280.

105 B. Z. Tang, H. Xu and W. Y. Lam, *Chem. Mater.*, 2000, **12**, 1446–1455.